A93-34123

AIAA-93-1592

Check for updates

EXPERIMENTAL UNSTEADY PRESSURES AT FLUTTER ON THE SUPERCRITICAL WING BENCHMARK MODEL

Bryan E. Dansberry, Michael H. Durham*, Robert M. Bennett**, José A. Rivera*, Walter A. Silva*, and Carol D. Wieseman*; Structural Dynamics Division, NASA Langley Research Center, Hampton, VA 23681-0001
and David L. Turnock*
Lockheed Engineering and Sciences Corporation

Downloaded by NASA LANGLEY RESEARCH CENTRE on September 29, 2020 | http://arc.aiaa.org | DOI: 10.2514/6.1993-1592

Abstract†

This paper describes selected results from the flutter testing of the Supercritical Wing (SW) model. This model is a rigid semispan wing having a rectangular planform and a supercritical airfoil shape. The model was flutter tested in the Langley Transonic Dynamics Tunnel (TDT) as part of the Benchmark Models Program, which is a multi-year wind tunnel activity currently being conducted by the Structural Dynamics Division of NASA Langley Research Center. The primary objective of this program is to assist in the development and evaluation of aeroelastic computational fluid dynamics codes. The SW is the second of a series of three similar models which are designed to be flutter tested in the TDT on a flexible mount known as the Pitch and Plunge Apparatus (PAPA). The PAPA provides a well defined two-degree-of-freedom dynamic system which allows rigid, instrumented models to undergo flutter in the TDT. Data sets acquired with these models, including simultaneous unsteady surface pressures and model response data, are meant to be used for correlation with analytical codes. Presented in this report are experimental flutter boundaries and corresponding steady and unsteady pressure distribution data acquired over two model chords located at the 60 and 95 percent span stations.

Nomenclature

a	speed of sound, ft/sec
b	model semichord, 8 inches
c	model chord, 16 inches
C_p	pressure coefficient, $(p-p_\infty)/q$
$\lvert C_p \rvert$	magnitude of oscillatory part of pressure measurements determined at the flutter frequency
f_2	wind-off pitch frequency, 5.25 Hz
f_f	flutter frequency, Hz
g	structural damping
k	reduced frequency, $b\omega/V$
l	wing span, 32 inches
m	calculated moving mass of PAPA/model system, 6.1 slugs
M	free-stream Mach number
p	measured pressure, psf
Phase	Phase angle referenced to pitch displacement
q	free-stream dynamic pressure, psf
R_n	Reynolds number based on chord length, c
V	free-stream velocity, ft/sec
V_I	flutter speed index, $V/b\omega(\mu^{-2})$
x	distance from wing leading edge, inches
x/c	fraction of chord length
y	distance from wing root, inches
Z	vertical plunge displacement, inches
α	wing angle of attack, degrees
α_m	mean wing angle of attack, degrees
θ	pitch displacement, degrees
μ	mass ratio, $m/\pi\rho l b^2$
ρ	density, slugs/ft^3
ω	circular frequency, rad/sec

Introduction

A significant number of aircraft aeroelastic problems occur in the transonic speed range. Classical flutter is of greatest concern at transonic Mach numbers. Non-classical instabilities such as buffet, control surface buzz, limit cycle oscillations, and shock induced oscillations are encountered in the transonic regime as well.

Aeroelastic analyses using computational fluid dynamics (CFD) codes hold promise for rational analysis of all these phenomena.[1] However, even for the classical flutter problem the assessment of CFD codes in the transonic region is far from complete. One handicap in the evaluation of CFD codes is the lack of well-documented experimental data sets. The development of aeroelastic CFD codes requires thorough experimental data sets to validate computed results and to guide the modification of newly developed analysis methods.

The Benchmark Models Program (BMP)[2] is being conducted by the Structural Dynamics Division of NASA Langley Research Center to assist in the development and evaluation of aeroelastic CFD codes. One way in which the BMP is attempting to accomplish this goal is through the generation of experimental data sets which incorporate simultaneous unsteady surface pressure and model response measurements at flutter. This is the purpose of testing the Supercritical Wing (SW) model.

The SW is the second of three rigid models scheduled to be flutter tested in the Langley Transonic Dynamics Tunnel (TDT) as part of the BMP. All three models are rigid semispan wings having an identical rectangular planform and identical instrumentation. The difference in these models is in their airfoil shape. The first model in this series had a NACA 0012 airfoil shape. Test results for this model are documented in references 3-5. The third model, to be tested later, has a NACA 64A010

---

*
**Member AIAA
Associate Fellow, AIAA

† Copyright c 1993 by the American Institute of Aeronautics and Astronautics, Inc. No copyright is asserted in the United States under Title 17, U.S. code. The U.S. Government has a royalty-free license to exercise all rights under the copyright claimed herein for Government purposes. All other rights are reserved by the copyright owner.

airfoil section. The SW model has a second generation supercritical airfoil section.

Like the other models in this series, the **SW** is designed to be flutter tested while mounted on the flexible Pitch and Plunge Apparatus **(PAPA).** The PAPA is used by the BMP to provide a well defined two-degrees-of-freedom dynamic system in which rigid models can flutter within the operating envelope of the TDT. Details of the wind-off dynamic characteristics of the model/PAPA system are documented in reference 6.

This paper presents an overview of the experimental data acquired from the flutter testing of the SW model. Flutter boundaries and aeroelastic model response data are presented, including flutter frequencies and mean amplitudes of plunge and pitch motion. Also, steady surface pressures, recorded with the model motion degrees of freedom locked out, and unsteady pressure distributions acquired during flutter are presented. In this paper the emphasis is placed on showing trends in the data using graphical representations of the results. This data will be documented in tabular form in a future NASA publication.

Apparatus

This section contains basic information about the SW model and associated test hardware. Wind-off dynamic characteristics of the two principle modes, rigid-body plunge and rigid-body pitch, are also presented. A more rigorous treatment of these subjects can be found in reference 6.

Wind Tunnel

Flutter testing of this model was conducted in the Langley Transonic Dynamics Tunnel (TDT).[7] The TDT is a continuous flow, single return wind tunnel with a 16-foot square test section (with cropped corners) having slots in all four walls. It is capable of operating at Mach numbers up to 1.2 and at stagnation pressures from near vacuum to atmospheric. The tunnel is equipped with 4 quick-opening bypass valves which can be used to rapidly reduce test section dynamic pressure and Mach number when an instability occurs. Either air or a heavy gas, R-12, can be used as the test medium. Both were employed for testing this model.

Model

The SW model is a rigid semispan wing model designed to be flutter tested on the flexible PAPA mount (described in another section). Figure 1 shows a photo of the model mounted in the test section. It has a simple rectangular planform with an SC(2)0414 second generation supercritical airfoil section. The model has a chord of 16 inches and **a** span of 32 inches giving it a panel aspect ratio of two. Beginning at the **32** inch span station, the model terminates in a tip-of-revolution where the radius is equal to half the airfoil thickness at each position along the chord.

Figure 1. Model in Test Section.

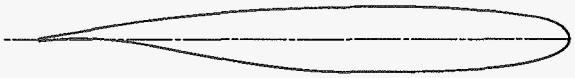

Figure 2. SC(2) 0414 Airfoil Section.

Figure 2 shows an outline of the SC(2)0414 supercritical airfoil section. This section was selected from several airfoils described in reference **8.** The "SC(2)" designation indicates it is part of the family of second generation supercritical airfoils, while the "0414" indicates that the airfoil section has a design lift coefficient of 0.4 and a maximum thickness of 14 percent of the chord.

The SW model contains 80 pressure transducers; 40 located to measure the surface pressure distribution at the 60 percent span station and 40 located to measure the surface pressure distribution at the 95 percent span station. The chordwise distribution of the pressure transducers is identical for both spanwise stations. There are 21 pressure orifices on the upper surface, one each at the leading and trailing edges, and 17 on the lower surface. The measured x/c locations for all 80 pressure orifices are presented in Table 1.

The pressure transducers used were differential pressure transducers rated for measurements up to 5 psid. In order to maintain phase relationships between pressure measurements, total transmission distance from surface orifice to pressure transducer was kept between 0.1 and 0.2 inches with only two exceptions. The two trailing edge pressure orifices required a metal tube to be run from the trailing edge forward to an area thick enough to house a pressure transducer. Transmission distance from trailing edge orifices to these pressure transducers was approximately 0.7 inches.

Reference pressure tubes from the 40 transducers located at each span station connected to a central manifold, which vented to an area of zero flow in the plenum of the wind-tunnel. Thus, each differential pressure transducer was referenced to free stream stagnation pressure.

Other model instrumentation included four low frequency accelerometers located near the four comers of

Downloaded by NASA LANGLEY RESEARCH CENTRE on September 29, 2020 | http://arc.aiaa.org | DOI: 10.2514/6.1993-1592

the model. These were used to verify flutter frequency and rigid body motion during testing. Also, two type "T," copper-constantin thermocouples were installed and positioned near the pressure transducers, one for each span station, so that the temperature history of each row of pressure transducers could be recorded.

Table 1. Measured locations of pressure orifices.

x/c for 60% Span		x/c for 95% Span	
Upper	Lower	Upper	Lower
0.000		0.000	
0.009	0.012	0.009	0.012
0.023	0.027	0.024	0.027
0.049	0.053	0.049	0.052
0.099	0.103	0.098	0.102
0.149		0.148	
0.198	0.203	0.198	0.203
0.249		0.248	
0.298	0.303	0.298	0.303
0.348		0.348	
0.398	0.403	0.398	0.403
0.448		0.448	
0.498	0.503	0.498	0.503
0.542	0.552	0.542	0.552
0.598	0.602	0.598	0.602
0.648	0.652	0.648	0.652
0.698	0.702	0.698	0.702
0.749	0.752	0.748	0.751
0.799	0.801	0.798	0.800
0.849	0.851	0.848	0.850
0.899	0.901	0.898	0.900
0.950	0.941	0.950	0.940
1.000		1.000	

Flexible Mount

The SW model was flutter tested on the Pitch and Plunge Apparatus (PAPA) flexible mount system.[9-10] A photo of the PAPA mount is presented in figure 3. The PAPA is used by the BMP to provide a well defined, two-degree-of-freedom dynamic system on which rigid, instrumented models can undergo flutter during in the TDT. It consists of a moving plate supported out from the tunnel wall by a system of four rods of circular cross-section and a centerline flat-plate drag strut; all having fixed-fixed end conditions. At the tunnel wall the rods and drag strut are attached to a mounting plate fixed to a turntable which allows remote angle-of-attack changes ($+4.8^o$ to -5.0^o) during wind-on testing. The moving plate can be considered rigid for the purposes of generating an analytical model, while the rods and flat plate drag strut provide linear elastic constraints such that the moving plate and attached model can oscillate in pitch and in plunge. The wind-off characteristics of these rigid-body pitch and plunge modes are determined by the length and cross-section of the rods as well as the mass of the moving plate and model. The main purpose of the drag strut is to increase stiffness in the x-y (chordwise) plane, moving the natural frequency of the first in-plane mode away from that of the plunge mode.

A top view sketch of the PAPA mount is presented in figure 4. As this illustration shows, ballast weights can be added to the inboard fore and aft portions of the moving plate. These weights are used to uncouple the wind-off pitch and plunge modes by moving the model/PAPA center of gravity forward or aft as necessary to locate it on the system elastic axis, which corresponds to the mid-chord of the model. Characteristics of the wind-off plunge and pitch modes of the model/PAPA system are provided in table 2. These modes dominate the flutter mechanism during wind-on testing. Further details on the wind-off dynamic characteristics of the model/PAPA system can be found in reference 6.

Instrumentation on the PAPA include strain gage bridges that are calibrated to measure vertical loading and vertical displacement, as well as torsional moment and pitch angle of the model. Mounted on the moving plate are two accelerometers to record pitch and plunge motion and an angle-of-attack accelerometer which is used to measure the static pitch angle of the moving plate.

Associated Hardware

As shown in figure 4, the PAPA mount is located behind a large splitter-plate when mounted in the tunnel test section. This splitter plate measures 12 feet in length and 10 feet in height and is suspended out from the tunnel wall by struts about 40 inches long. Behind the splitter-plate, the PAPA mount is isolated from the free-stream flow in an aerodynamic fairing. The splitter-plate serves to separate the model from flow about the aerodynamic fairing as well as from the tunnel wall boundary layer.

The model is attached to the PAPA moving plate by means of a short pedestal block that protrudes through an opening in the splitter-plate. The opening is large enough to allow the PAPA/model assembly to translate several inches in the vertical direction without contacting the splitter-plate. Flow through the splitter-plate is prevented by a thin, circular, end-plate, one model chord length in diameter, which is mounted between the pedestal and model. This end-plate covers the opening in the splitter-plate and is recessed such that the end-plate outer surface coincides with the surface of the splitter-plate to preserve smooth aerodynamic flow. The inner surface of the end-plate is not allowed to rub against the recessed surface of the splitter-plate. The top-view sketch of figure 4 shows how the PAPA, splitter-plate, model, and other components fit together. The model and end-plate mounted in front of the splitter plate in the test section can be seen in figure 1. Figure 5 shows a picture of the model, splitter plate, and PAPA mount assembled in the test section.

Downloaded by NASA LANGLEY RESEARCH CENTRE on September 29, 2020 | http://arc.aiaa.org | DOI: 10.2514/6.1993-1592

Table 2. Wind-off characteristics of primary modes.

	Frequency	Stiffness	Structural Damping, g	Generalized Mass
Plunge	3.32 Hz	2637 lb/ft	0.002	6.1 slugs
Pitch	5.25 Hz	2964 ft-lb/rad	0.002	2.7 slug-ft^2

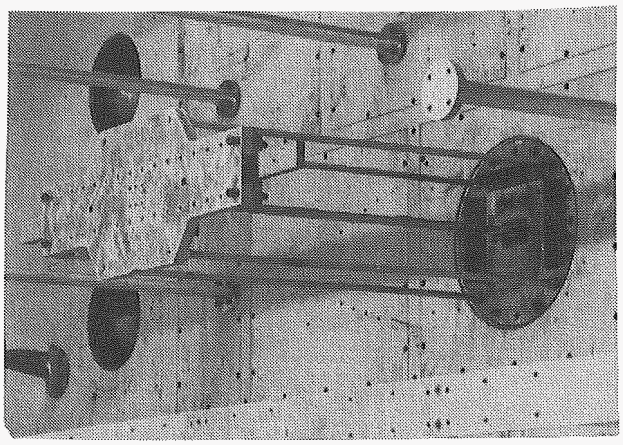

Figure 3. Photograph of PAPA.

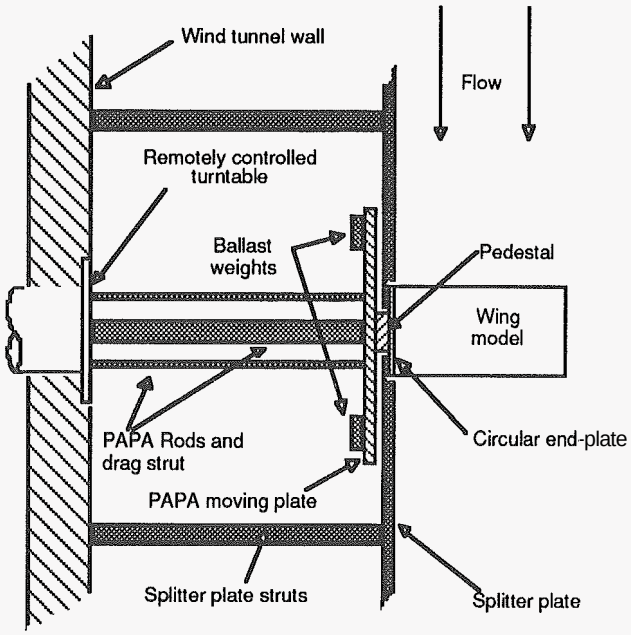

Figure 4. Top-view sketch of PAPA.

The splitter plate was instrumented for some surface pressure measurements. These measurements provide data on the aerodynamic conditions at the model root plane which could be used to check boundary conditions for CFD analysis. A total of 20 pressure transducers of the same type used in the model were located along two vertical and one horizontal rows. Also, a boundary layer rake was mounted on the splitter plate at a point one chord length behind and above the trailing edge of the model. In this rake, ten pressure transducers were used to measure the stagnation pressure at points ranging from 0.25 to 5 inches from the surface of the splitter plate. This information provides an estimate of the thickness of the splitter plate boundary layer. Results of the measurements on the splitter plate are not documented here, but will be included in a future NASA report.

Data Acquisition & Reduction

Time history data were acquired for 122 channels of data using the TDT data acquisition system. These data included 80 pressure transducers and two thermocouples on the model, 20 pressure transducers on the splitter-plate, and 10 pressure transducers on the boundary layer rake. Dynamic response data included four accelerometers on the model, two accelerometers on the PAPA mount, two strain gauge bridges on the PAPA (oriented for pitch and for plunge), and two angle-of-attack accelerometers, one on the PAPA moving plate and one on the turntable. Data from all channels were acquired simultaneously (not multiplexed) at a rate of 500 samples per second for 20 seconds and stored in digital form on disk. A 200 Hz low pass filter system was employed to avoid aliasing.

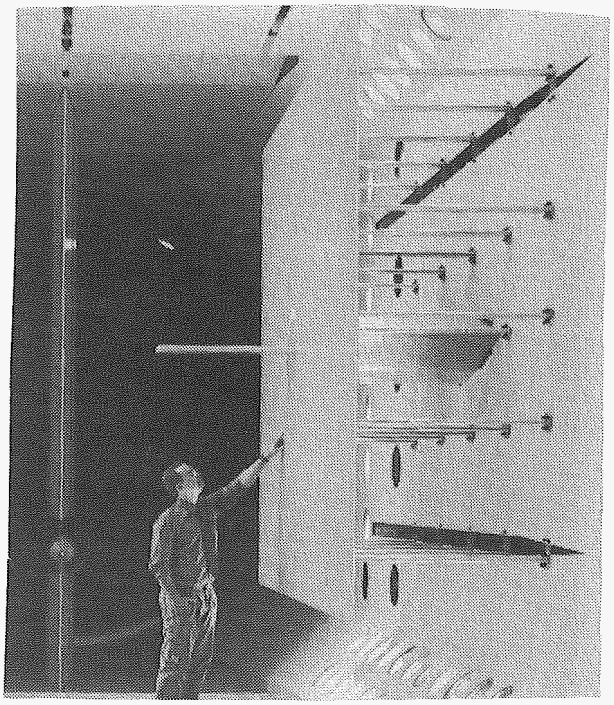

Figure 5. Model, PAPA, and splitter plate in test section.

The bending and torsion strain gauge bridges on the PAPA mount were calibrated to obtain plunge position and pitch angle time histories of the SW model relative to the turntable. The turntable angle was recorded by an angle-of-attack accelerometer. From these data channels,

Downloaded by NASA LANGLEY RESEARCH CENTRE on September 29, 2020 | http://arc.aiaa.org | DOI: 10.2514/6.1993-1592

flutter frequency, model mean angle of attack, and the magnitude of oscillations in both plunge and pitch were calculated for each flutter data point.

For each differential pressure transducer the mean pressure was calculated using all 10,000 samples of data. This mean was divided by the dynamic pressure, q, at which the data was recorded to form a mean pressure coefficient, C_p. In order to examine the unsteady portion of the pressure measurements, a discrete Fourier analysis at the flutter frequency was used to determine magnitude and phase. In order to compare between test conditions, these magnitude results were normalized by the magnitude of the oscillating pitch angle. Phase of the unsteady portion of the pressures were determined relative to the pitch motion. These phase results are positive in value when the oscillatory signal leads the wing pitch motion.

Table 3. Experimental results in air with free. transition

Tab Point no.	α_m deg	M	q lb/ft^2	a ft/sec	V ft/sec	ρ slugs/ft^3	R_n x10^{-6}	μ	V_I	f_f Hz	f_f/f_2	k	Z Mag in.	Z Phase deg	θ Mag deg
72	-0.1	.32	140.3	1142.2	364.4	.002113	1.988	776	.68	4.60	.88	.0529	.21	-175.4	1.05
57	0.0	.51	152.2	1129.6	574.7	.000922	1.391	1779	.73	4.47	.86	.0326	.21	-176.3	0.86
141	-0.2	.73	172.4	1120.2	817.6	.000516	1.122	3569	.83	4.23	.81	.0217	.59	-176.6	1.47
133	0.0	.77	168.9	1115.6	857.6	.000459	1.055	3178	.82	4.14	.80	.0202	.44	-176.3	0.94
74	1.0	.33	145.1	1140.2	372.0	.002097	2.019	782	.70	4.55	.88	.0513	.26	-175.1	1.23
60	1.0	.51	156.4	1130.4	580.0	.000930	1.415	1763	.74	4.43	.85	.0320	.28	-175.8	1.12
139	1.2	.72	170.2	1121.1	812.4	.000516	1.113	3180	.82	4.19	.81	.0216	.71	-175.7	1.94
137	1.2	.77	169.3	1117.8	856.8	.000461	1.054	3556	.84	4.09	.79	.0200	.82	-175.4	1.92

Table 4. Experimental results in air with fixed transition using #30 grit.

Tab Point no.	α_m deg	M	q lb/ft^2	a ft/sec	V ft/sec	ρ slugs/ft^3	R_n x10^{-6}	μ	V_I	f_f Hz	f_f/f_2	k	Z Mag in.	Z Phase deg	θ Mag deg
280	0.1	.34	157.1	1140.1	384.8	,002122	2.113	773	.73	4.54	.87	.0494	.53	-175.3	2.53
272	-0.1	.53	168.5	1135.2	598.2	.000942	1.468	1741	.77	4.45	.86	.0311	.38	-176.7	1.34
267	0.0	.62	169.2	1130.0	706.2	.000679	1.258	2416	.78	4.40	.85	.0261	.35	-176.8	1.10
265	0.0	.71	172.6	1121.2	797.5	.000543	1.150	3020	.80	4.34	.83	.0228	.36	-177.5	1.01
212	0.0	.72	175.8	1121.3	812.4	.000533	1.150	3077	.81	4.29	.83	.0221	.47	-177.3	1.22
208	0.0	.78	173.3	1116.8	866.0	.000462	1.070	3548	.83	4.20	.81	.0203	.23	-177.0	0.51
211	1.0	.72	172.3	1120.7	803.2	.000534	1.141	3069	.81	4.29	.82	.0224	.45	-177.0	1.20
206	1.1	.78	172.4	1115.7	864.9	.000461	1.067	3556	.83	4.18	.80	.0203	.46	-177.1	0.99

Table 5. Experimental results in air with fixed transition using #35 grit.

Tab Point no.	α_m deg	M	q lb/ft^2	a ft/sec	V ft/sec	ρ slugs/ft^3	R_n x10^{-6}	μ	V_I	f_f Hz	f_f/f_2	k	Z Mag in.	Z Phase deg	θ Mag deg
341	0.0	.34	155.5	1138.6	381.9	.002132	2.112	769	.72	4.55	.87	.0499	.25	-175.8	1.09
333	-0.2	.50	160.1	1132.2	569.5	.000987	1.471	1660	.75	4.47	.86	.0329	.37	-176.7	1.37
329	-0.4	.62	168.2	1124.5	696.9	.000693	1.277	2366	.78	4.39	.84	.0264	.57	-177.0	1.74
321	-0.1	.68	171.1	1123.1	763.0	.000588	1.188	2789	.79	4.36	.84	,0239	.37	-177.0	1.08
319	-0.1	.74	177.6	1117.7	825.0	.000522	1.149	3142	.82	4.27	.82	,0217	.51	-176.8	1.26
315	-0.1	.76	173.8	1115.8	850.8	.000480	1.094	3413	.82	4.23	.81	.0208	.31	-177.5	0.73

Table 6. Experimental results in R-12 with fixed transition using #35 grit.

Tab Point no.	α_m deg	M	q lb/ft^2	a ft/sec	V ft/sec	ρ slugs/ft^3	R_n x10^{-6}	μ	V_I	f_f Hz	f_f/f_2	k	Z Mag in.	Z Phase deg	θ Mag deg
492	-0.3	.44	157.4	506.5	220.4	.006482	5.268	253	.72	4.53	.87	.0861	.28	-172.5	1.20
488	-0.2	.58	162.4	508.0	294.2	.003752	4.075	437	.75	4.45	.86	.0633	.29	-174.0	1.03
485	-0.2	.69	169.3	507.9	350.0	,002764	3.579	593	.79	4.35	.84	.0521	.49	-174.7	1.42
480	-0.1	.74	168.8	5M.6	375.7	.002392	3.340	685	.79	4.30	.83	.0480	.38	-175.2	1.01
465	0.0	.80	172.6	510.9	407.4	.002080	3.113	788	.84	4.14	.80	.0425	.70	-173.9	1.40
472	0.0	.80	170.7	510.0	409.3	.002038	3.072	805	.83	4.15	.80	.0424	.37	-174.8	0.73
457	1.3	.80	166.9	509.7	407.3	.002012	3.022	815	.82	4.14	.80	.0425	.35	-174.5	0.69
470	0.0	.82	178.8	511.5	417.7	.002050	3.141	800	.87	4.05	.78	.0407	.62	-173.4	1.01
466	0.0	.82	177.5	510.0	419.7	.002016	3.116	813	.85	4.13	.79	.0412	.24	-174.5	0.42
427	5.4	.80	1'24.7	507.2	406.1	.001512	2.281	1084	.60	4.87	.94	.0503	.08	-162.9	0.69
403	5.3	.80	105.5	505.6	404.0	.001293	1.951	1268	.55	4.89	.94	.0507	.05	-168.0	0.43
395	5.5	.80	93.6	503.6	402.0	.001158	1.749	1416	.51	4.97	.96	.0518	.08	-167.5	0.90

Downloaded by NASA LANGLEY RESEARCH CENTRE on September 29, 2020 | http://arc.aiaa.org | DOI: 10.2514/6.1993-1592

Downloaded by NASA LANGLEY RESEARCH CENTRE on September 29, 2020 | http://arc.aiaa.org | DOI: 10.2514/6.1993-1592

Discussion of Results

Flutter Boundaries

Two different **types** of instability boundaries were defined during testing: conventional and stall. Conventional flutter boundaries were defined for a model initial angle of attack of zero using both air and R-12 as a test medium. The second type of instability boundary, stall flutter, was defined at one Mach number by a few flutter points at model mean angles of attack ranging from 0.0 to 5.5 degrees. The test conditions and flutter parameters, including the magnitude and phase of the pitch and plunge displacement during flutter, for each test point on these flutter boundaries are presented in Tables 3-6.

In air the boundaries were defined with and without fixed boundary layer transition. To fix the transition point a grit strip, 0.25" in width, running from root to tip on both the upper **and** lower surfaces was used. Two fixed transition configurations and one free transition configuration were tested in air. In R-12 only one configuration was tested. It had fixed transition.

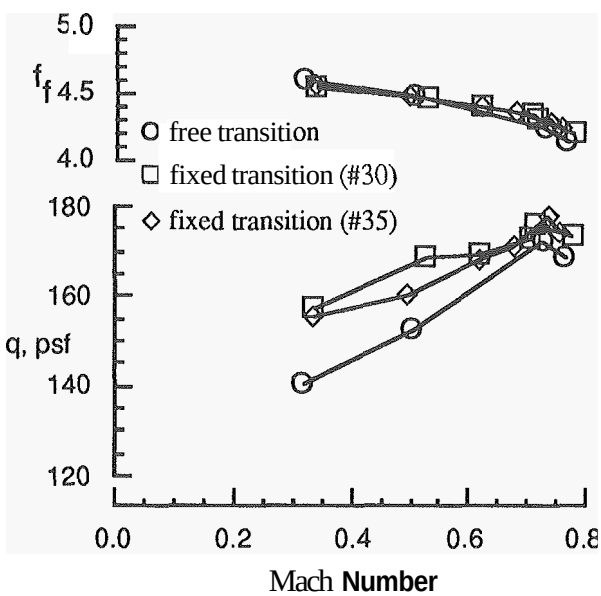

Figure 6. Transition effects on conventional flutter boundary in air (α_m=0°).

Conventional flutter- The conventional flutter boundary was defined in both air and R-12 and for fixed and free transition. These boundaries are presented in figures ***6-8*** **as** flutter dynamic pressure, **q,** versus Mach number. In these figures the model/PAPA system is stable below the boundary and unstable above the boundary. Also included are plots of flutter frequency, f_f, versus Mach number. Flutter frequency for these boundaries varies from near 4.5 Hz at subsonic Mach numbers to around 4.1 Hz in the transonic regime, indicating strong participation of both the plunge and pitch modes of the PAPA/model system.

In the subsonic region, the **q** versus Mach number boundaries show the unusual trend of increasing flutter dynamic pressure with increasing Mach number. This is likely the result of the system elastic axis and center of gravity being located at the wing mid-chord. Also, the transonic dip for these boundaries is shallow and centered near Mach 0.76.

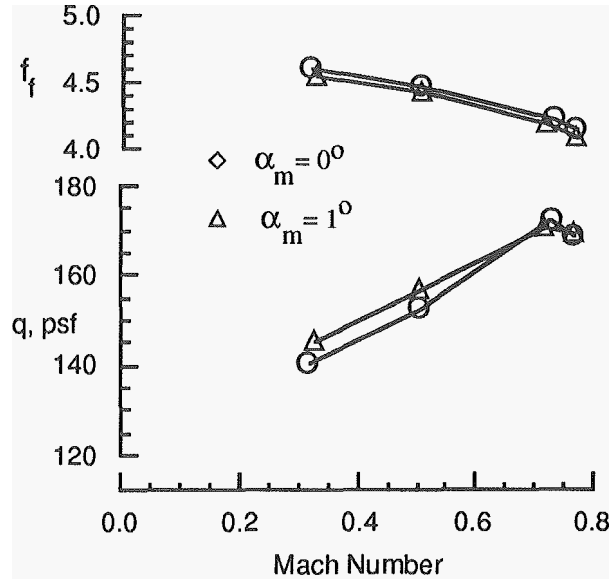

Figure 7. α_m effects on free transition flutter boundary in air.

Figure 6 shows the effects on the flutter boundary in air of fixing the point on the model where the boundary layer transitions from laminar to turbulent. As mentioned previously, two different fixed transition configurations were tested. In both cases the transition point was fixed at 6.5 percent chord on both the upper and lower surfaces. The difference in the two configurations was a change in grit size from #30 to #35. Also, the transition strip used for the #35 grit configuration was wrapped around the tip while the #30 configuration left transition free on the tip. As can be seen in the figure, the main effect of fixing the transition point was to increase the flutter dynamic pressure. This effect is greater at subsonic Mach numbers than at transonic Mach numbers. The two transition fixed configurations show no significant differences.

Figure 7 shows the effects of a one degree change in initial angle of attack on the flutter boundary. These data were recorded in air with free transition. The effects on the flutter boundary are small.

Figure **8** shows the effects of testing in air and R-12 on the flutter boundary for a fixed transition configuration. (All data in R-12 was acquired using the #35 transition strip.) At the same Mach number **and** dynamic pressure, testing in R-12 increases Reynolds number by a factor of 3 and decreases mass ratio by a factor of 5. The effects on the flutter boundary are noticeable only in the transonic regime, where the flutter dynamic pressure is reduced slightly.

Stall flutter- Additional flutter points were acquired at non-zero angles of attack at a constant Mach number of

0.8. These data, acquired in 11-12 with fixed transition, are presented in figure 9 as flutter dynamic pressure versus α. The test conditions and flutter parameters for these stall flutter points are included in table 6.

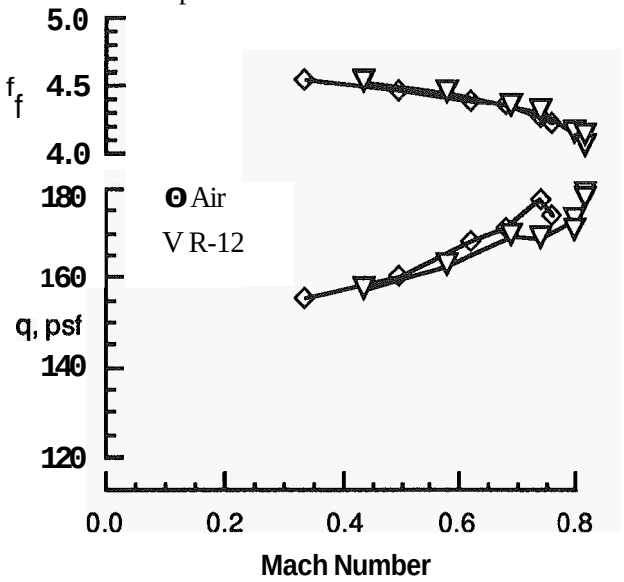

Figure 8. Flutter boundaries in air and R-12 for fixed transition (#35 grit).

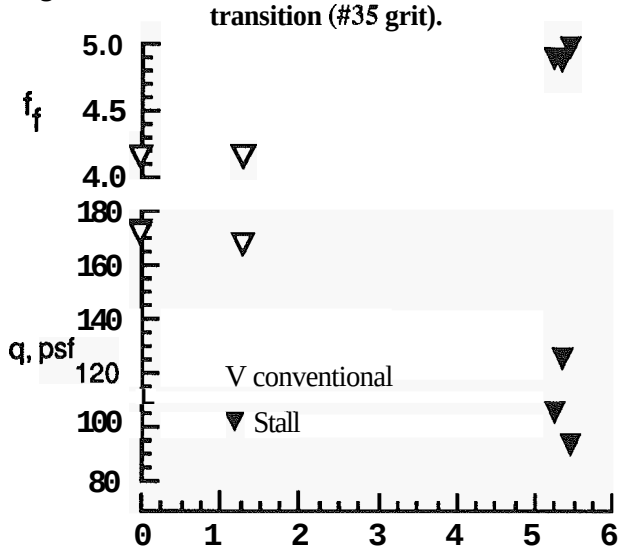

Figure 9. Stall flutter boundary in R-12 at M = 0.80.

Due to load limits of the PAPA mount only three points could be acquired at angles of attack greater than two degrees. The data acquired, however, shows trends consistent with those of models previously tested on the PAPA mount. Results for models previously tested on the PAPA mount show that the flutter dynamic pressure varies only slightly as α is increased to some critical angle (above four degrees in reference 4). At this point, a rapid decrease in flutter dynamic pressure with increasing angle of attack and a rise in the flutter frequency to very near the wind-off torsion frequency is seen[4]. This rapid change in character from equal participation in the flutter mechanism of pitch and plunge to a pitch dominated flutter mechanism is associated with wing stall conditions during a portion of the pitch oscillation cycle.

Pressure Measurements

Unsteady surface pressure data were recorded while the model was experiencing flutter. Unsteady pressure measurements were recorded over a continuous 20 second period at each of the flutter points shown in figures 6-9. The flutter motion involved sinusoidal plunge and pitch motion of nearly constant amplitude throughout the 20 seconds of data acquisition. Figures 10-13 show selected unsteady pressure distribution results.

Steady pressure data were acquired with the PAPA mount system plunge and pitch degrees of freedom locked so that the model was held in a fixed position. Measurements taken while the model was held fixed were obtained in both air and R-12 at Mach numbers identical to those at which flutter data were recorded and at angles of attack ranging from -3 to +4.8 degrees. All rigidized data were acquired using the #35 grit fixed transition configuration. Figure 13 compares one set of steady pressure data with unsteady data recorded at identical Mach and q conditions.

Figure 10(a) shows the steady portion of the pressure distributions at both the 60 and 95 percent span locations in terms of mean pressure coefficient, C_p, and the difference in C_p from upper to lower surface, ΔC_p. These data were recorded in R-12 at Mach numbers near the transonic dip of the flutter boundary. As can be seen in all the ΔC_p plots presented, mean or static loads on this airfoil section are almost entirely generated aft of the mid-chord line. Also, moving from 60 to 95 percent span does show a slight decrease in the loads generated. Figure 10(b) shows the magnitude, $|C_p|$, normalized by the pitch amplitude, and the phase of the oscillatory portion of these pressure measurements at the flutter frequency only. Oscillatory loads on the model are largely generated ahead of the mid-chord line. However, there is some loading evident in the cusp region at the 60 percent span station. This loading appears to wash out near the tip since it is not evident at the 95 percent span station. At the highest Mach number there is also some loading and a phase change on the lower surface of the model centered around the mid-cord. This loading also appears to wash out near the tip since it is not evident at the 95 percent span station and could be associated with a shock formation which is strongest at the center of the model span and weakest near the root and tip. Flow visualization results have indicated the possibility of this type of shock formation.

Figure 11(a) shows the mean C_p and ΔC_p distributions recorded in air for all three model transition configurations at nearly identical subsonic conditions. Figure 11(b) shows the magnitude and phase of the oscillatory portion of these pressure measurements at the flutter frequency. These distributions show the effects on a subsonic pressure distribution of fixing transition. One noticeable effect is an increase in the aft loading for the free transition case. This change in loading is evident in the cusp region at both span stations.

Downloaded by NASA LANGLEY RESEARCH CENTRE on September 29, 2020 | http://arc.aiaa.org | DOI: 10.2514/6.1993-1592

Downloaded by NASA LANGLEY RESEARCH CENTRE on September 29, 2020 | http://arc.aiaa.org | DOI: 10.2514/6.1993-1592

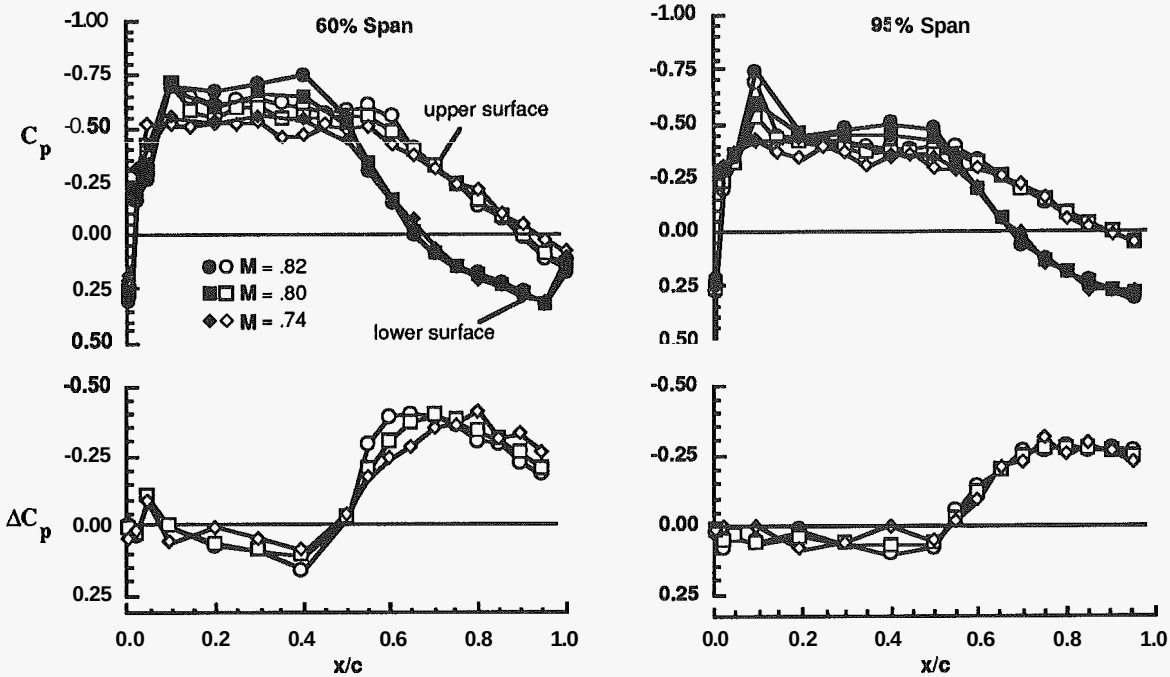

Figure 10(a). Mean portion of pressure distributions recorded during flutter.

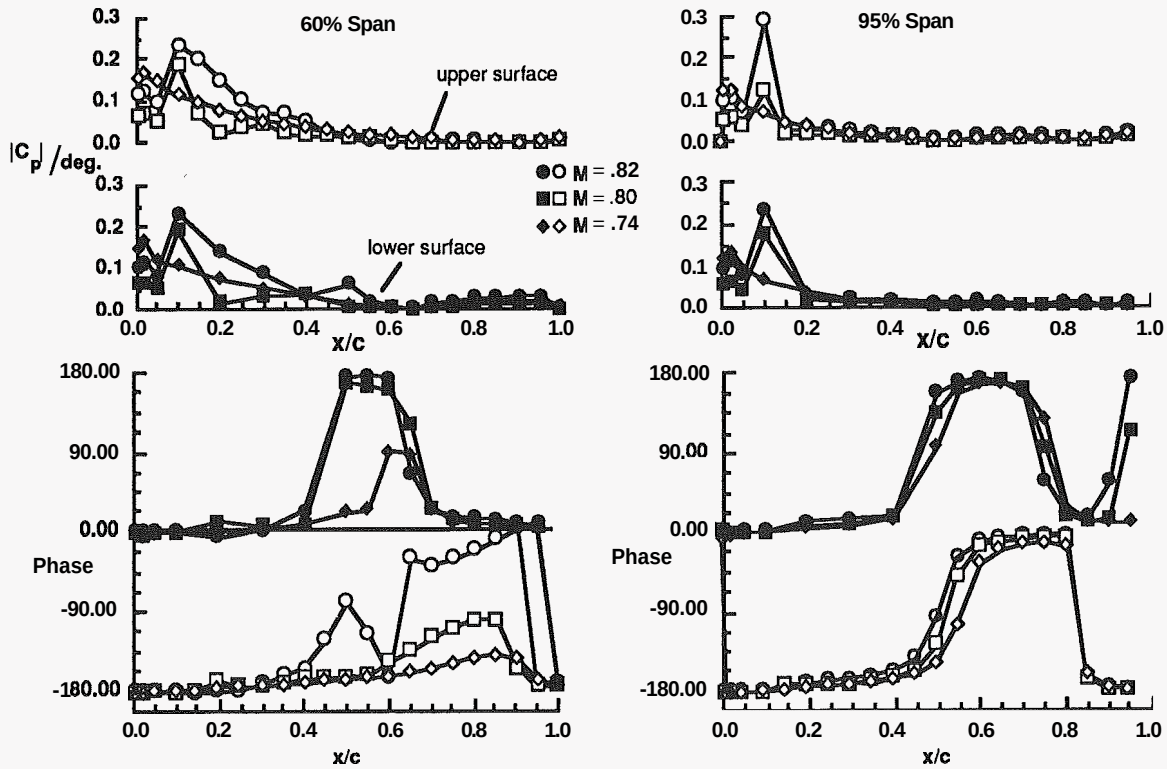

Figure 10(b). Unsteady portion of pressure distributions recorded during flutter

Figures 10. Transonic Mach effects in R-12 with transition fixed

Figures 12(a) and 12(b) show mean C_p and ΔC_p of the pressure data, and magnitude and phase of the oscillatory portion of the pressure distributions recorded in air for all three model transition configurations at nearly identical transonic conditions. Comparing these distributions shows the effects on a transonic pressure distribution of fixing transition. As in the subsonic case, there is an increase in the aft loading, evident in the cusp region, for the free transition case. Another effect can be seen in the data corresponding to 0.1 x/c where a spike in the magnitudes of both the mean and oscillatory portions of the pressure can be seen in the fixed transition results. This pressure "spike" is of nearly equal strength at both span stations and is not evident in the subsonic data.

Because it appears at the first measurement location aft of the transition strip, it may indicate a separation bubble created by the transition strip. This effect appears to be localized to the first five percent chord aft of transition and is similar to results found in references **4** and 5.

Figure **13** shows the mean pressure distributions at M = 0.74 recorded in air and R-12. It also shows the steady pressure distribution recorded with the model/PAPA system degrees of freedom locked out. There are no significant differences in these pressure distributions.

Concluding Remarks

The Benchmark Models program, currently being conducted by the Structural Dynamics Division of NASA Langley Research Center, has the primary objective of assisting in the development and evaluation of aeroelastic computational fluid dynamics codes. This paper described the experimental data set acquired from the flutter testing of the Supercritical Wing (SW) model.

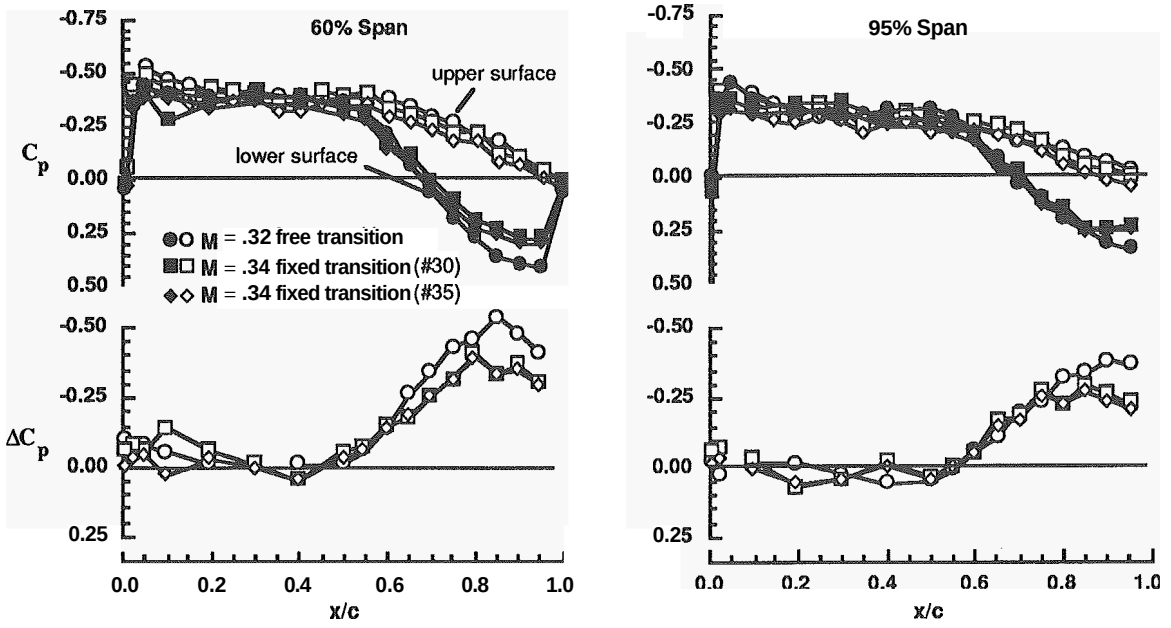

Figure 11(a). Mean portion of pressure distributions recorded at flutter.

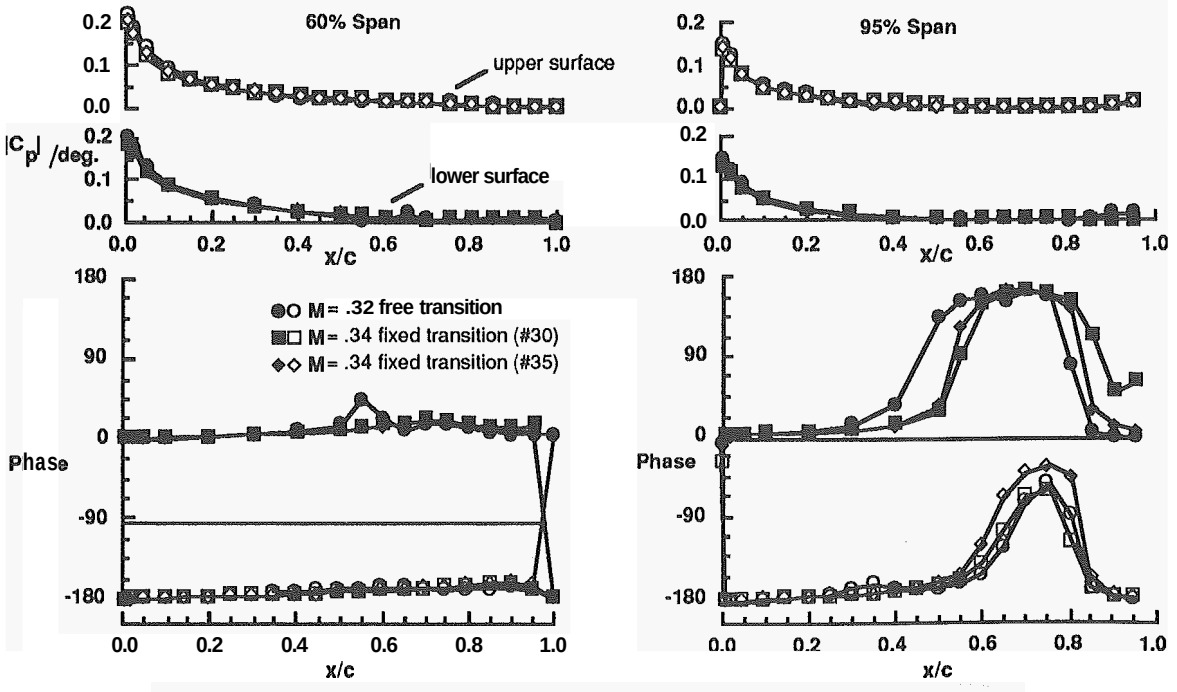

Figure 11(b). Unsteady portion of pressure distributions recorded at flutter.

Figures 11. Transition effects in air at low Mach numbers.

Downloaded by NASA LANGLEY RESEARCH CENTRE on September 29, 2020 | http://arc.aiaa.org | DOI: 10.2514/6.1993-1592

Downloaded by NASA LANGLEY RESEARCH CENTRE on September 29, 2020 | http://arc.aiaa.org | DOI: 10.2514/6.1993-1592

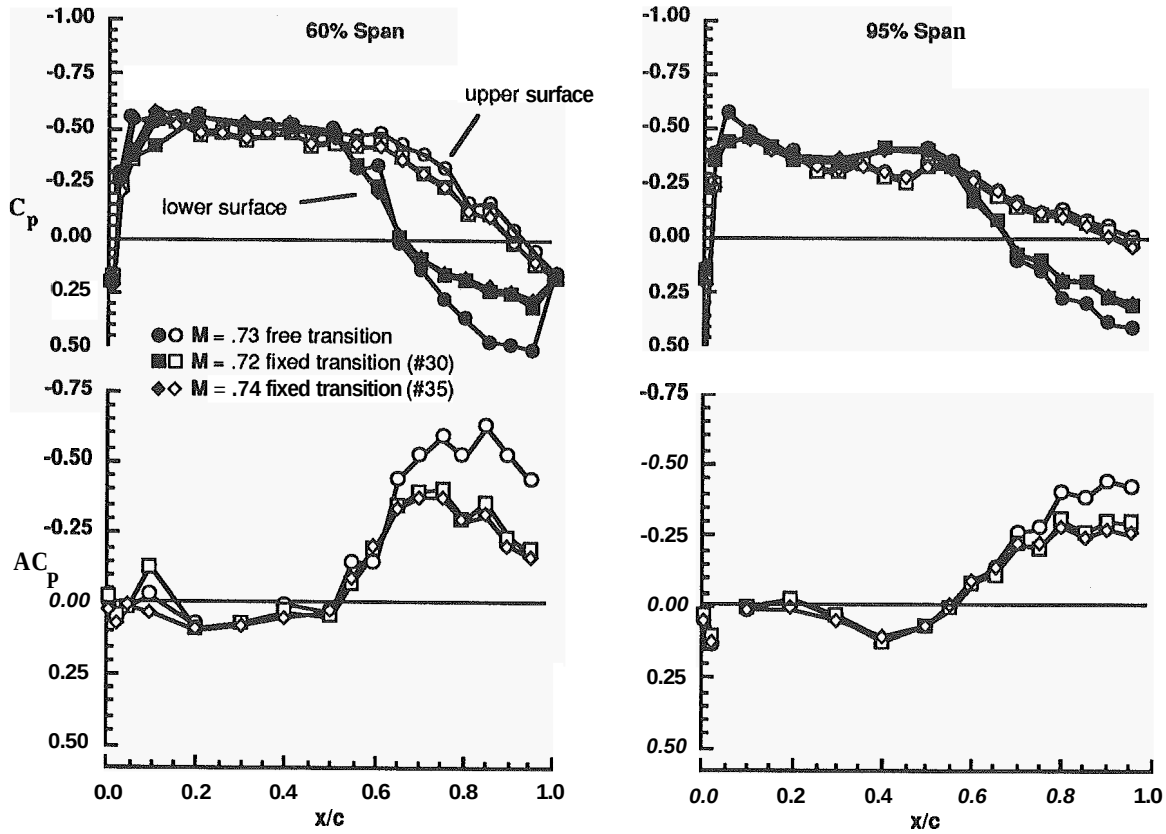

Figure 12(a). Mean portion of pressure distributions recorded at flutter.

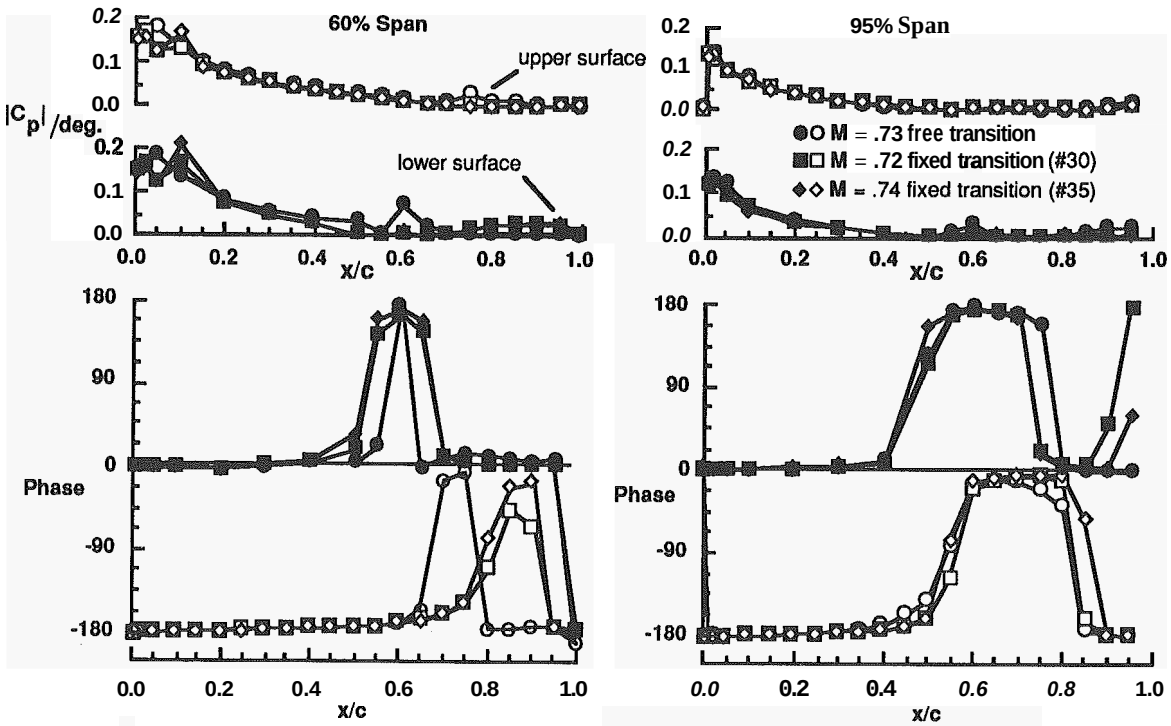

Figure 12(b). Unsteady portion of pressure distributions recorded during flutter

Figures 12. Transition effeets at transonic conditions in air.

The SW model is a rigid semispan model with a rectangular planform and a supercritical airfoil shape. The model was flutter tested in the Langley Transonic Dynamics Tunnel (TDT) on a flexible mount known as the Pitch and Plunge Apparatus (PAPA). The PAPA mount provides a two degrees-of-freedom dynamic

system in which the model can move in both rigid-body plunge and rigid-body pitch. Some details of the dynamic characteristics of these pitch and plunge modes were provided in this report. Further details can be found in reference 6.

The SW model is the second of a series of three similar models which are designed to be flutter tested in the TDT on the PAPA mount. Data presented in this report includes experimental flutter boundaries and corresponding unsteady pressure distribution data acquired over two model chords, both upper and lower surface, located at the 60 and 95-percent span stations. Current activities include further evaluation of the surface pressure measurements with the goal of making this data available, in tabular as well as graphical form, for aeroelastic CFD code development and evaluation.

References

1. Edwards, J. W.; and Malone, J. B.: "Current Status of Computational Methods for Transonic Unsteady Aerodynamics and Aeroelastic Applications", Paper No. 25, AGARD Specialists Meeting on Aerodynamics and Aeroelasticity, San Diego, CA, October 9-11, 1991.

2. Bennett, R.M.; Eckstrom, C.E.; Rivera, J.A., Jr.; Dansberry, B.E.; Farmer, M.G.; and Durham, M. H.: "The Benchmark Aeroelastic Models Program - Description and Highlights of Initial Results", NASA TM 104180, December 1991.

3. Rivera, J.A.; Dansberry, B.E.; Farmer, M.G.; Eckstrom, C.V.; Seidel, D.A.; and Bennett, R.M.: "Experimental Flutter Boundaries with Unsteady Pressure Distributions for the NACA 0012 Benchmark Model", AIAA Paper No. 91-1010, April, 1991. Also NASA TM-104072, 1991.

4. Rivera, J.A.; Dansberry, B.E.; Bennett, R.M.; Durham, M. H.; and Silva, W. A.: "NACA 0012 Benchmark Model Experimental Flutter Results with Unsteady Pressure Distributions", AIAA Paper No. 92-2396, April, 1992. Also NASA TM-107581, 1992.

5. Rivera, J.A.; Dansberry, B.E.; Durham, M. H.; Bennett, R.M.; and Silva, W. A.: "Pressure Measurements on a Rectangular Wing with a NACA 0012 Airfoil During Conventional Flutter", NASA TM-104211, 1992.

6. Dansberry, B.E.; Durham, M. H.; Bennett, R.M.; Turnock, David L.; Silva, W. A.; and Rivera, J.A.: "Physical Properties of the Benchmark Models Program Supercritical Wing", NASA TM 4457, February, 1993.

7. Reed, Wilmer H.: "Aeroelasticity Matters: Some Reflections on Two Decades of Testing in the NASA Langley Transonic Dynamics Tunnel", NASA TM-83210, 1981.

8. Harris, C. D.: "NASA Supercritical Airfoils", NASA TP 2969, March, 1990.

9. Farmer, M. G.: " A Two-Degree-of-Freedom Flutter Mount System with Low Damping for Testing Rigid Wings at Different Angles of Attack", NASA TM-83302, 1982.

10. Farmer, M. G.: " Model Mount System for Testing Flutter", U. S. Patent Number 4,475,385, October 9, 1984.

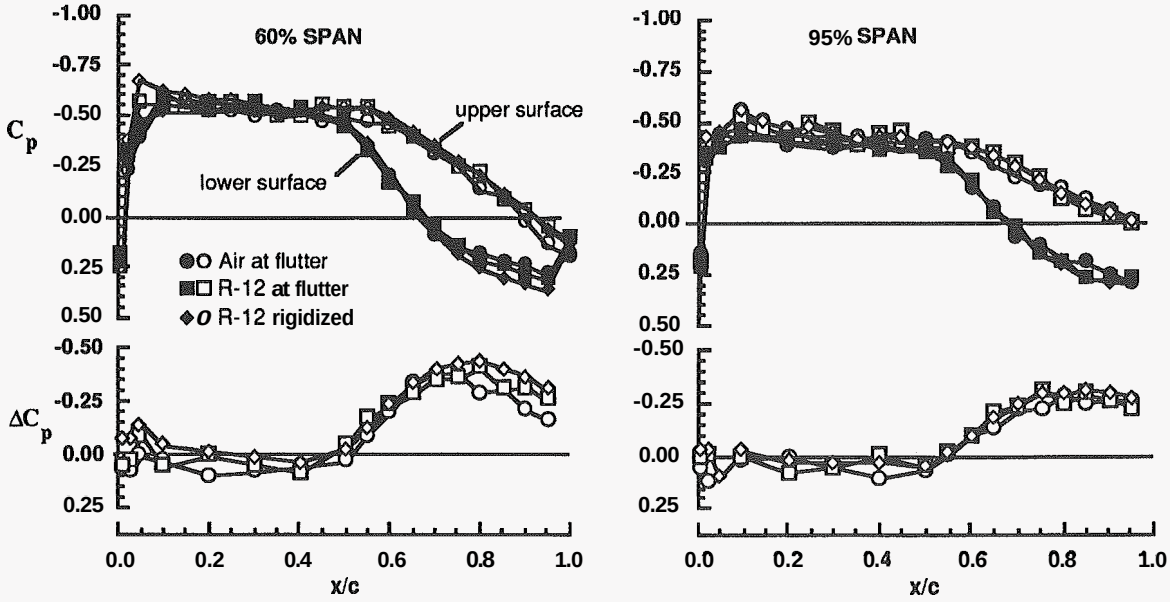

Figure 13. Comparison of mean pressures in air and R-12 and steady pressures in R-12 for M = 0.74.

Downloaded by NASA LANGLEY RESEARCH CENTRE on September 29, 2020 | http://arc.aiaa.org | DOI: 10.2514/6.1993-1592